Comparative study of the electronic structure of $(SN)_x$ and its precursor S_2N_2 using the extended tight-binding method

I. P. Batra, S. Ciraci,* and W. E. Rudge
IBM Research Laboratory, San Jose, California 95193
(Received 31 January 1977)

We present detailed electronic structure, total density of states, and orbital density of states for polymeric sulfur nitride $(SN)_x$, and disulfur dinitride S_2N_2, using the extended tight-binding method. To our knowledge this is the first time that S_2N_2 has been investigated in any detail from the electronic-structure point of view. By a comparative study of S_2N_2 and $(SN)_x$, S-3p and N-2p hybridization increases leading to a charge delocalization and hence enhanced conductivity. This is a direct consequence of the novel structure of $(SN)_x$. We have also been able to provide a complete interpretation of the ultraviolet and x-ray photoelectron spectra of $(SN)_x$. The intensities of various peaks are in good accord with those expected from our calculated symmetries of initial-state wave functions. Similar data are provided for S_2N_2 with the hope that the experimental results will be forthcoming.

I. INTRODUCTION

During the recent past there has been a tremendous growth of interest in polymeric sulfur nitride,[1-7] $(SN)_x$, and other substances[8,9] containing SN as its constituents. An understanding of the origin of metallic conductivity and superconductivity in the inorganic polymer $(SN)_x$ has been an important topic of investigation. This has spurred much interest in theoretical electronic-structure calculations.[10-19] These include various one-dimensional model calculations and several three-dimensional calculations using empirical and first-principles methods. Fully three-dimensional first-principles calculations for this system are rather difficult (and expensive) because it contains eight atoms in the unit cell. Nevertheless, outstanding efforts by various workers[10-19] have resulted in a great deal of understanding about the nature of bands for $(SN)_x$. Most calculations are in good overall agreement in the valence-band region, but differ (in varying degrees) from each other in the region near the Fermi surface. No electronic band-structure calculation for the crystalline disulfur dinitride (S_2N_2) has thus far been presented. Since $(SN)_x$ crystals are usually grown via the solid-state polymerization of single crystals of S_2N_2, an understanding of the electronic structure of S_2N_2 may provide valuable insight into the origin of metallic conductivity for $(SN)_x$. Therefore it is important to study both these systems in a comparative fashion within the same set of approximations.

In this paper we present the electronic structure for $(SN)_x$ as well as its precursor S_2N_2, calculated using the extended tight-binding method.[20,21] This is a first-principles method with no fitting or adjustable parameters introduced into the calculation. Our method is practically identical to the one used by Ching and Lin.[19] There are, however, differences in details which will be pointed out subsequently. We have investigated the basis-set dependence of the band structure. The effect of including d orbitals for sulfur is also studied.

For the first time, we predict that S_2N_2 is an indirect-gap semiconductor. Of course, in agreement with earlier experiments and calculations, we find that $(SN)_x$ is metallic in nature. The nature of this distinction between the two materials is discussed later in terms of bonding effects. For this purpose we are going to describe in detail the orbital composition of various energy bands for $(SN)_x$ and S_2N_2. The results are also presented for total and orbital density of states for $(SN)_x$ and S_2N_2. Using our calculated orbital density of states we have been able to provide a complete interpretation of the ultraviolet and x-ray photoemission spectra for $(SN)_x$. We hope similar experiments will soon be performed on S_2N_2.

II. METHOD OF CALCULATION

We used the extended tight-binding method[20,21] and employ a Slater-type expression for the exchange potential ($\alpha = \frac{2}{3}$). In this method the one-electron wave function for the system having three-dimensional periodicity can be expressed as a linear combination of Bloch sums

$$\psi_n(\vec{k},\vec{r}) = \sum_\mu a_{\mu n}(\vec{k}) X_\mu(\vec{k},\vec{r}) \ , \tag{1}$$

where the Bloch sums X_μ are constructed in the usual manner

$$X_\mu(\vec{k},\vec{r}) = [N\Omega_\mu(\vec{k})]^{-1/2} \sum_\nu e^{i\vec{k}\cdot(\vec{R}_\nu+\vec{\tau}_\mu)} \phi_\mu(\vec{r}-\vec{R}_\nu-\vec{\tau}_\mu). \tag{2}$$

Here N is the number of lattice sites in the crystal (and the summation is over all N of these sites), $\vec{R}_\nu$ are the direct-lattice translation vectors, and $\vec{\tau}_\mu$ are nonprimitive translation vectors for the atoms in the unit cell. $\Omega_\mu(\vec{k})$ is the normalization factor for the Bloch sums $\langle X_\mu | X_\mu \rangle = 1$ and $\phi_\mu(\vec{r} - \vec{R}_\nu - \vec{\tau}_\mu)$ represents an appropriate basis orbital centered at $\vec{R}_\nu + \vec{\tau}_\mu$. In what follows, we will restrict ourselves to Gaussian-type orbitals and thus ϕ_μ consists of a single Gaussian or a linear combination of Gaussians (contracted basis set). An analytical evaluation of the various matrix elements can be carried[20] out for such a basis set.

The expansion coefficients in Eq. (1) are obtained using the variational principle

$$\frac{\partial}{\partial a_\mu(\vec{k})}\left[\frac{\langle\psi|H|\psi\rangle}{\langle\psi|\psi\rangle}\right]=0, \quad \mu=1,2,3,\ldots,M, \tag{3}$$

where M is the number of different kinds of orbitals used in the trial wave function. This leads to the secular equation

$$\det\left|H_{\mu,\mu'}(\vec{k}) - E(\vec{k})S_{\mu,\mu'}(\vec{k})\right| = 0. \tag{4}$$

For M basis orbitals in the unit cell, the secular equation is an algebraic function of the Mth degree for E, which therefore has M roots for a given $\vec{k}$. The advantage[21,22] of the extended tight-binding method lies in the fact that M is usually much smaller than, say, the matrix to be diagonalized in the orthogonalized-plane-wave method[18] to obtain comparable accuracy. The matrix elements between μ and μ' for an operator Θ are defined as

$$\Theta_{\mu,\mu'}(\vec{k}) = \frac{1}{[\Omega_\mu(\vec{k})\Omega_{\mu'}(\vec{k})]^{1/2}} \times \sum_\beta e^{i\vec{k}\cdot(\vec{R}_\beta+\vec{\tau}_{\mu'}-\vec{\tau}_\mu)} \times \int \phi_\mu^*(\vec{r}-\vec{\tau}_\mu)\Theta\phi_{\mu'}(\vec{r}-\vec{R}_\beta-\vec{\tau}_{\mu'})\,d\vec{r}. \tag{5}$$

By setting Θ equal to $1, -\nabla^2, V(\vec{r})$ in Eq. (5) one, respectively, gets expressions for the overlap, kinetic energy and potential energy matrix elements. The kinetic energy and overlap matrix elements ($S_{\mu,\mu'}$) over the Gaussian basis can be evaluated analytically and efficiently. To ensure accuracy, the β summation in Eq. (5) is truncated only after sufficient neighbor interactions (typically 5–6) have been included. The potential energy integrals, which are multicenter in nature, deserve some further discussion.

The crystal potential in the overlapping atomic potential model can be expressed as

$$V_T(\vec{r}) = \sum_{\nu,\mu}\left(-\frac{2Z_\mu}{r_{\nu\mu}} + V_H(r_{\nu\mu}) + V_X(r_{\nu\mu})\right), \tag{6}$$

where $r_{\nu\mu} = |\vec{r} - \vec{R}_\nu - \vec{\tau}_\mu|$, V_H and V_X are the Hartree and exchange potentials respectively, and Z_μ is the atomic number of the μth atom. If we attempted to expand the above potential in a Fourier series, a huge number of reciprocal-lattice vectors $\vec{G}$ would be required to adequately represent the core part. Therefore we use an Ewald type of procedure,[22-24] where the slowly convergent core potential $V_C(\vec{r})$ is expressed in terms of Gaussian functions centered at each atomic site, i.e.,

$$V_C(\vec{r}) = \sum_{\nu,\mu}\left(\frac{C_1(\mu)}{r_{\nu\mu}}e^{-a_1(\mu)r_{\nu\mu}^2} + \frac{C_2(\mu)}{r_{\nu\mu}}e^{-a_2(\mu)r_{\nu\mu}^2} + \sum_{i=3}^{m} C_i(\mu)e^{-a_i(\mu)r_{\nu\mu}^2}\right). \tag{7}$$

The coefficients C_i and exponents a_i are obtained through a least-squares-fitting procedure. Furthermore, to get a very accurate description of the core region, an additional restriction is placed on the first two coefficients, namely, $C_1(\mu) + C_2(\mu) = -2Z_\mu$. One then writes

$$V_T(\vec{r}) = V_C(\vec{r}) + V_S(\vec{r}), \tag{8}$$

where $V_S(\vec{r})$ is a very smooth function and can thus be readily expanded in a rapidly convergent Fourier series

$$V_S(\vec{r}) = \sum_{\vec{G}} V_S(\vec{G})e^{-i\vec{G}\cdot\vec{r}}. \tag{9}$$

The matrix elements of $V_C(\vec{r})$ can be calculated analytically in direct space and the matrix elements of $V_S(\vec{r})$ are evaluated using the generalized overlap matrix.[25] It should be noted that the decomposition of the total potential into core and smooth potentials is only for computational convenience. Furthermore, by choosing an appropriate value for m in Eq. (7), one may be able to make $V_S(\vec{G})$ negligibly small and thus carry out all matrix elements evaluation in direct space. Our calculation differs from an earlier linear-combination-of-atomic-orbitals (LCAO) calculation[19] in the treatment of potential, the choice of basis set, and the treatment of core states.

Let us now illustrate the above procedure for the cases of $(SN)_x$ and S_2N_2. To generate the crystalline potential, we first need atomic potentials for sulfur and nitrogen atoms which are themselves generated from self-consistent Hartree-Fock atomic-charge densities.[26] These atomic-charge densities are shown in Fig. 1 by placing S and N atoms 3.0 a.u. (approximately the S-N bond length) away from each other. We assumed the configurations $S(1s^2 2s^2 2p^6 3s^2 3p^4)\,^3P$ and $N(1s^2 2s^2 2p^3)\,^4S$ in evaluat-

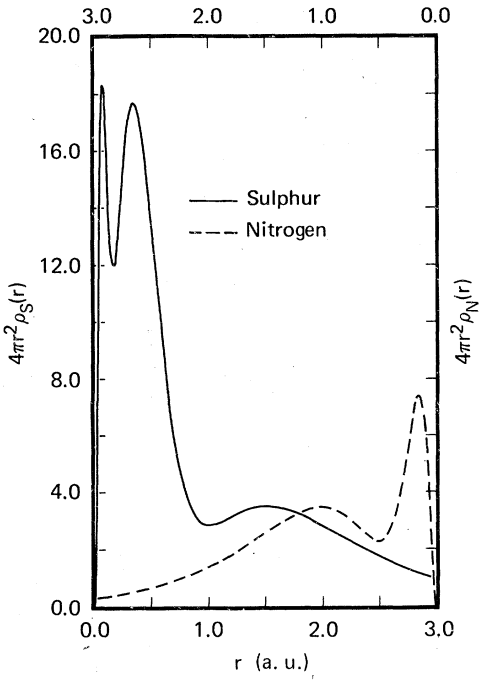

FIG. 1. Self-consistent atomic charge densities for sulfur (solid line) and nitrogen (dashed line) atoms used for generating crystalline potential.

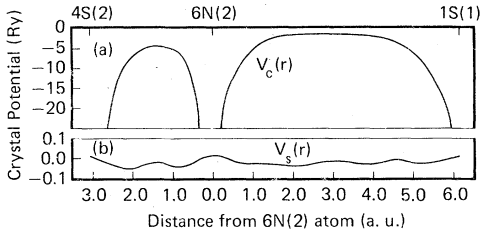

FIG. 2. (a) Rapidly varying core potential $V_C(\vec{r})$ and (b) smooth part of the crystalline potential $V_S(\vec{r})$ along two particular directions in $(SN)_x$.

ing charge densities from the double-ζ Slater functions.[26] The atomic potentials were obtained from these charge densities using $\alpha = \frac{2}{3}$ for the exchange term. These atomic potentials were then cast in a Gaussian form according to Eq. (7). Excellent representation from the atomic potentials was obtained by choosing $m = 9$ for S and $m = 8$ for N. The potential exponents and coefficients for S and N are given in Table I. To appreciate how well the Gaussian representation is able to describe the actual crystalline potential, we have plotted $V_C(\vec{r})$ and $V_S(\vec{r})$ in Fig. 2 along two particular directions in $(SN)_x$. By comparing the scales in Figs. 2(a) and 2(b), one concludes that $V_S(\vec{r})$ is going to make only a small contribution to potential matrix elements. We have ensured rapid convergence of the Fourier series in Eq. (9) because $V_S(\vec{r})$ is a smoothly varying function of $\vec{r}$.

Next we need to establish the basis set. We tried three different sets[27] (a) S(8/5), N(6/4); (b) S(8/7), N(6/5); (c) S(8/7/1), N(6/5). Here the notation $A(u/v/w)$ means that for an atom A we used u Gaussians of s-type, v Gaussians of p-type, and w Gaussians of d-type. A general Gaussian function at site $\vec{P}$ is defined by[27]

$$G(\vec{r}) = (x - P_x)^l (y - P_y)^m (z - P_z)^n \exp(-\alpha r_P^2). \tag{10}$$

The orbital exponents α, for S and N for the three basis sets are given in Table II. The $3d$-orbital component for S was optimized by Roos and Siegbahn[27] for the H_2S molecule. The electronic band-structure along a particular direction (ΓZ) in the Brillouin zone for various basis sets is shown in Fig. 3. In all cases we retained up to sixth-neighbor interactions in direct space.

The most noticeable effect of using the extended basis set (b) is to lower the unoccupied conductions bands around 4 eV by about 0.5 eV. Further inclusion of d orbitals on sulfur (basis set c) depresses the low-lying valence bands by about 1 eV. The contribution of the d orbitals in any given energy

TABLE I. Gaussian description of potential for sulfur and nitrogen atoms.

	Sulfur		Nitrogen	
i	Exponents a_i(S)	Coefficients C_i(S)	Exponents a_i(N)	Coefficients C_i(N)
1	5916.0786	−1.9726	66.8414	2.8042
2	112.2558	−30.0274	15.2716	−16.8042
3	193.2946	162.8773	25.0229	50.3238
4	37.4901	−120.0104	4.9335	−14.7361
5	11.5035	−57.5661	1.6408	−7.4592
6	3.2643	−23.6092	0.5617	−2.3352
7	0.8166	−8.0929	0.1606	−0.6976
8	0.2186	−1.6811	0.0604	−0.1575
9	0.0530	−0.3749	...	...

TABLE II (a). Gaussian basis sets (exponents) for sulfur atom.

S(8/5)		S(8/7)		S(8/7/1)	
s	*p*	*s*	*p*	*s,p*	*d*
881.6767	31.5219	same	212.8659	same	0.54[a]
251.5860	9.3515	as	49.6002	as	
80.7947	2.9701	used	15.5155	used	
27.6606	0.6525	in	5.4756	in	
6.0144	0.1806	the	2.0442	the	
2.2986		S(8/5)	0.5218	S(8/7)	
0.4342		set	0.1506	set	
0.1608					

(b). Gaussian basis sets (exponents) for nitrogen atom.

N(6/4		N(6/5)	
s	*p*	*s*	*p*
226.3050	13.5731	same	26.8690
60.3599	2.9231	as	5.9912
16.7189	0.7989	used	1.7508
5.1331	0.2189	in	0.5606
0.7809		the	0.1759
0.2374		N(6/4)	
		set	

[a] For this choice of the polarization exponents see Roos and Seighbahn (Ref. 27).

state was ≤5%. Similar conclusions have been arrived at by Salaneck *et al.*[8] from S_4N_4 molecular studies. They[8] report S-3*d* contributions in the range of 0–4% for various molecular orbitals. By examining Fig. 3, we conclude that for our comparative study the changes due to use of extended basis may be ignored. Further, we are purposely restricting ourselves to atomically-contracted basis-sets because we are interested in tracing the orbital composition of various energy levels. The effect of introducing additional variational freedom by decontraction leads[19] to a somewhat better description for the unoccupied bands, which are not our primary interest here. Our programs are not capable of performing the calculations self-consistently at the present time. However, all previous calculations on $(SN)_x$ are non-self-consistent and have correlated rather well with experiments. Therefore our hope is that for a comparative study of $(SN)_x$ and S_2N_2, both performed within the same set of approximations, the lack of self-consistency is not a serious limitation.

III. RESULTS AND DISCUSSION

In this section we present the results for the electronic structure of $(SN)_x$ and S_2N_2. But more importantly our emphasis is going to be on the orbital character of various parts of the energy bands. We feel this information gives insight

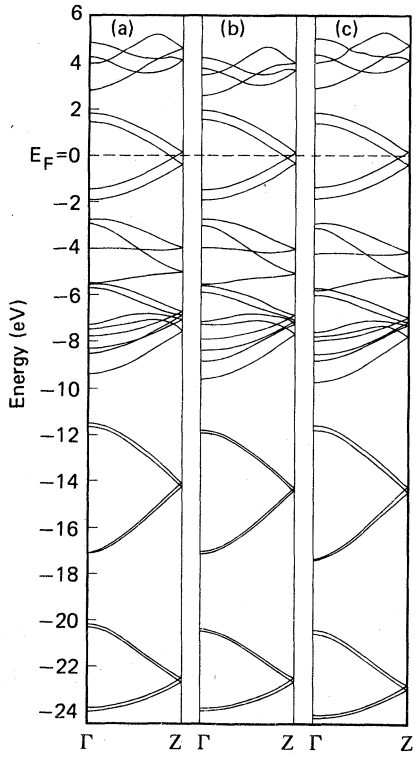

FIG. 3. Electronic energy band structure of $(SN)_x$ along the intrachain direction (ΓZ) for various basis sets (a) S(8/5), N(6/4); (b) S(8/7), N(6/5); (c) S(8/7/1), N(6/5).

into the nature of bonds. Armed with this knowledge for both the materials, one can attempt to understand why they behave so differently in their electrical properties.

The nature of the bands can be conveniently discussed by decomposing the total density of states (TDOS) into local or orbital density of states. The weight of the μth Bloch sum in the wave function corresponding to the eigenvalue $E_n(\vec{k})$ can be conveniently defined as[21,23,24]

$$f_{\mu n}(\vec{k}) = \sum_{\mu'} a^*_{\mu n}(\vec{k}) a_{\mu' n}(\vec{k}) S_{\mu,\mu'}(\vec{k}) \Big/ \sum_{\mu}\sum_{\mu'} a^*_{\mu n}(\vec{k}) a_{\mu' n}(\vec{k}) S_{\mu,\mu'}(\vec{k}) \ . \tag{11}$$

If the wave function (1) is normalized, then the denominator in Eq. (11) is unity. Furthermore, since the overlap matrix is Hermitian, one can write

$$f_{\mu n}(\vec{k}) = |a_{\mu n}(\vec{k})|^2 + \sum_{\mu' \neq \mu} \mathrm{Re}[a^*_{\mu n}(\vec{k}) a_{\mu n}(\vec{k}) S_{\mu,\mu'}(\vec{k})] \ . \tag{12}$$

The orbital density of states can now be defined as[24,28]

$$O_\mu(E) = \frac{1}{\sigma(2\pi)^{1/2}} \sum_{n,\vec{k}} f_{\mu n}(\vec{k}) \exp\left(\frac{-[E - E_n(\vec{k})]^2}{2\sigma^2}\right), \tag{13}$$

where each eigenvalue has been Gaussian broadened by σ (halfwidth at half-maximum). One could selectively sum various $f_{\mu n}(\vec{k})$ to learn about the s, p, d character of the state (orbital composition). We carry out such an analysis below. For clarity of presentation let us discuss $(SN)_x$ and S_2N_2 in separate subsections.

A. $(SN)_x$

The crystal structure used in our calculations is based on the work of Mikulski *et al.*[29] The atomic positions of four sulfur and four nitrogen atoms belonging to the monoclinic unit cell (space group $P2_1/c$) are listed in Table III. We retained interactions between atoms separated by up to 16 a.u. This amounted to including up to sixth-neighbor interaction. Other parameters of the calculation have been discussed earlier. The resulting band structure along various symmetry directions using the basis set (a) is shown in Fig. 4. The insert in Fig. 4 shows the projection of the Brillouin zone in the $k_y = 0$ plane.

We get a total valence bandwidth of about 24 eV (found by accommodating 44 valence electrons) and our overall band structure agrees rather well with other first principle three-dimensional calculations.[14,17-19] Our calculated bandwidth is to be compared with the experimental value of 24.4 $\pm$0.7 eV reported by Ley.[30] The bands are highly dispersive along the chain direction (see, for example, ΓZ direction), but the bands along the interchain direction (say ZE and ZD) are quite flat. This is consistent with the observation that $(SN)_x$ exhibits highly anisotropic properties. The interchain coupling is responsible for lifting the degeneracies along the ΓZ direction. At the Z point, the splitting near the Fermi level (E_F) is 0.54 eV and the Fermi level lies just slightly above the crossing point along ΓZ. From the location of E_F

TABLE III. Unit-cell geometry for $(SN)_x$.[a]

Center name[b]	x	y	z
1S(1)	−2.37181	2.41006	−1.39785
2S(2)	2.37181	−2.41006	1.39785
3S(1)	−5.01702	−1.78427	−3.17263
4S(2)	5.01702	1.78427	3.17263
5N(1)	−2.65259	−0.57882	−1.61915
6N(2)	2.65259	0.57882	1.61915
7N(1)	−4.73624	−4.77314	−2.95132
8N(2)	4.73624	4.77314	2.95132
$\vec{a}$	7.38883	0.0	−2.64566
$\vec{b}$	0.0	8.38866	0.0
$\vec{c}$	0.0	0.0	14.43212

[a] All distances are in atomic units; $\vec{a}, \vec{b}, \vec{c}$ are primitive translation vectors in direct space.

[b] The number in parentheses identifies the chain on which the atom is located.

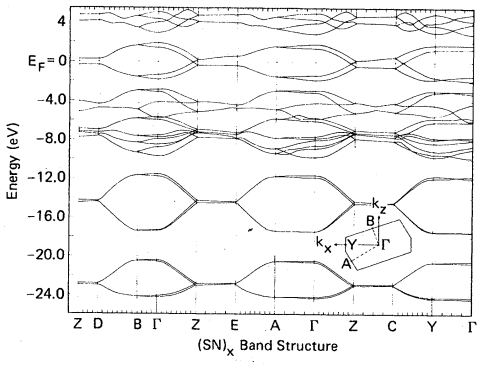

FIG. 4. Electronic energy band structure of $(SN)_x$ along various directions in the Brillouin zone. The inset shows the projection of the Brillouin zone in the $k_y = 0$ plane.

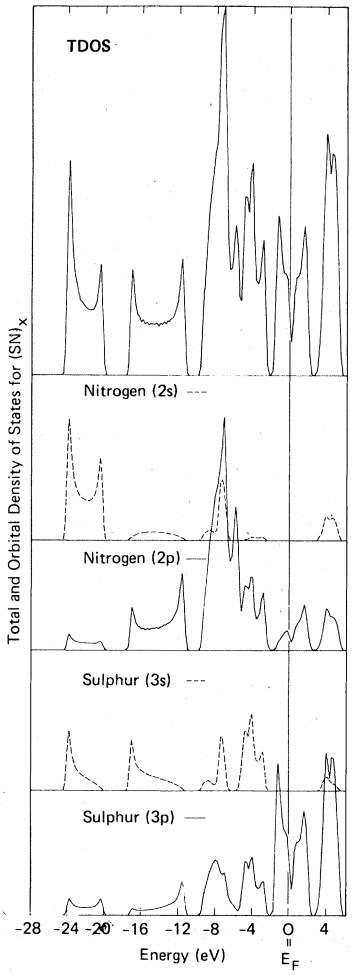

FIG. 5. Total and orbital density of states (normalized with respect to TDOS) for $(SN)_x$.

in Fig. 4, we expect to find a small electron pocket near Z. Since the Fermi level lies slightly below the crossing point along the CY direction, a small hole pocket is expected near C. It is noted that the location of E_F, using energy broadening procedure (0.15-eV halfwidth) which we have employed, is slightly uncertain. Our results near E_F differ from the orthogonalized-plane-wave bands,[18] where much larger electron- and hole-pockets are expected. In this region we are in closer agreement with other three-dimensional calculations based on empirical pseudopotentials,[14] extended Huckel[17] and LCAO[19] schemes. Contrary to Kamimura *et al.*[16] but in agreement with several[14,17,19] other calculations, we tend to conclude that the absence of Peierls distortion in $(SN)_x$ is due to the strong three-dimensional character of the solid. The origin of the difference between our results and Kamimura *et al.* findings may lie in an inappropriate choice of parameters by the latter group.

It may be remarked that most of our findings are in excellent agreement with those reported by Ching and Lin[19] using an LCAO method. At first sight this is not unexpected since we are also using an extended tight-binding scheme. However, since there are differences in our implementation of the tight-binding method, and we have done the elaborate computer programming completely independently, it is gratifying for us to obtain results for $(SN)_x$ which closely agree with the earlier calculation.[19]

The character of various bands can be conveniently presented by plotting the total and orbital density of states as shown in Fig. 5. We stress that the region near the Fermi energy consists of states having their origin in S $3p$ and N $2p$. This is a point of distinction between $(SN)_x$ and S_2N_2. We believe that S $3p$ and N $2p$ hybridization leads to delocalization of charge carriers and is in a qualitative sense responsible for the conductive properties of $(SN)_x$. The orbital composition of the state distribution can also provide a reasonable interpretation of x-ray[30,31] and ultraviolet[32] photoelectron spectra (XPS and UPS) because of the initial-state effects. A detailed analysis is presented below.

Figure 6 compares our calculated TDOS with the XPS results obtained by two different experimental groups.[30,31] Both groups utilized monochromatic x rays (Al $K\alpha$, 1486.6 eV). The spectra reported by Ley[30] contains five main pieces of structure labeled $L1$ through $L5$ [Fig. 6(a)] centered at 21.0, 15.2, 7.4, 3.6, and 0.7 eV, respectively, below E_F. Mengel *et al.*[31] report six peaks labeled $M1$, $M2$, $M2'$, $M3$, $M4$, and $M5$ in Fig. 6 (b) centered at 21.5, 16.5, 13.2, 7.5, 4.0 and 1.0 eV, respectively, below E_F. They[31] are thus able to resolve the $L2$ peak seen by Ley[30] into two components $M2$ and $M2'$. The two spectra are quite consistent with respect to the location of various peaks. However, there are obvious differences in the intensities of the various peaks especially when the substrate or background contributions are subtracted from the raw data. Our calculated density of states are shown in Fig. 6(c). We used a Gaussian broadening parameter $\sigma = 0.15$ eV. The centers of our main peaks labeled $B1$ through $B5$ are located at 22.4, 14.4, 7.1, 4.1, and 0.9 eV, respectively, below E_F. It should be noted that we are predicting a lot of structure in the $B4$ region which we are assuming is not resolved in the above XPS works. In fact our calculation predicts at least four peaks in the region starting at 3 eV below E_F and extending to about 11 eV below E_F. In recent UPS experiments on polycrystalline film and single crystal of $(SN)_x$, Koch and Grobman[32]

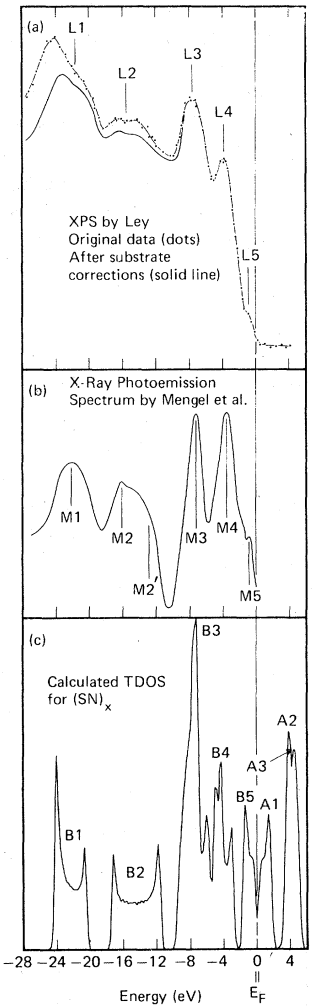

FIG. 6. Comparison of our calculated total density of states with the XPS results obtained by two different experimental groups (a) XPS results by Ley (Ref. 30) (b) XPS results by Mengel *et al* (Ref. 31). (c) Our calculation.

report four distinct peaks or shoulders in this energy range. This region is heavily derived from N $2p$ and S $3p$ states. It is usual for UPS experiments to provide better resolution than XPS in this energy range.

We can make some qualitative statements about the intensities of various peaks in XPS and UPS studies because we have at our disposal the symmetries of the initial-state wave functions. To predict intensities accurately one of course needs the matrix elements and the convolution with the final density of states. As seen from Fig. 5, the N $2s$ electrons are mainly responsible for the low-lying band $L1$. The $L2$ structure arises from an admixture of N $2p$, S $3s$, and s $3p$ states, and has lower intensity than $L1$. This intensity difference has been interpreted by noting[30] that the atomic photoelectric cross-section ratios σ(N $2s$):σ(S $3s$) are about 5:1. However, we feel that since the peak $L2$ does contain a considerable N $2p$ character, the XPS intensity for this band is likely to be low because of negligible photoionization cross section.[33] In fact, our calculation shows that the lower portion of the $L2$ band is S $3s$ rich and the upper portion is (N $2p$)+(S $3p$) rich (see Fig. 5). Such character can be responsible for the asymmetric peak which is reported by Mengel *et al.*[31] [peaks $M2$ and $M2'$ in Fig. 6(b)]. The $L3$ peak is expected to have lower intensity than indicated by our calculation because of considerable N $2p$ character in this band for which the photoionization cross section is very low[33] at 1500 eV. The $L4$ peak is observable with intensity nearly identical to $L3$ [see peaks $M3$ and $M4$ is Fig. 6(b)] because of the S $3s$ electrons. The band $B5$ near E_F is due to (S $3p$)+(N $2p$). Since σ(S $3p$):σ(S $3s$) is about 1:4 and σ(N $2p$)$\to 0$ at x-ray energies,[33] the peak $L5$ (or $M5$) is observed only as a shoulder. Our calculated width of the conduction band [$B5$ in Fig. 6(c)] is 1.7 eV. This value is to be compared with the experimental estimate[30] of 1.6 $\pm$0.3 eV for the width of the conduction band. The finite density of states at E_F gives $(SN)_x$ its metallic character.

B. S_2N_2

Disulfur dinitride[29,34,35] forms in a monoclinic crystal with two S_2N_2 molecules per unit cell. The space group is $P2_1/c$, the same as for $(SN)_x$. The geometrical positions for the eight atoms in the crystalline unit cell given in Table IV are based on

TABLE IV. Unit-cell geometry for S_2N_2.[a]

Center name[b]	x	y	z
1S(1)	1.64565	0.86137	−2.77969
2S(2)	−1.64565	4.42074	2.77969
3S(1)	−1.64565	−0.86137	−5.20644
4S(2)	1.64565	2.69800	5.20644
5N(1)	−1.41047	0.33814	−2.33450
6N(2)	1.41047	3.89751	2.33450
7N(1)	1.41047	−0.33814	−5.65164
8N(2)	−1.41047	3.22123	5.65164
$\vec{a}$	8.12949	0.0	−2.39727
$\vec{b}$	0.0	7.11874	0.0
$\vec{c}$	0.0	0.0	15.97227

[a] All distances are in atomic units; $\vec{a}, \vec{b}, \vec{c}$ are primitive translation vectors in direct space.

[b] The number in parentheses identifies the molecular unit number on which the atom is located. Thus atoms 1, 3, 5, and 7 constitute one S_2N_2 molecular unit and atoms 2,4,6,8 the other.

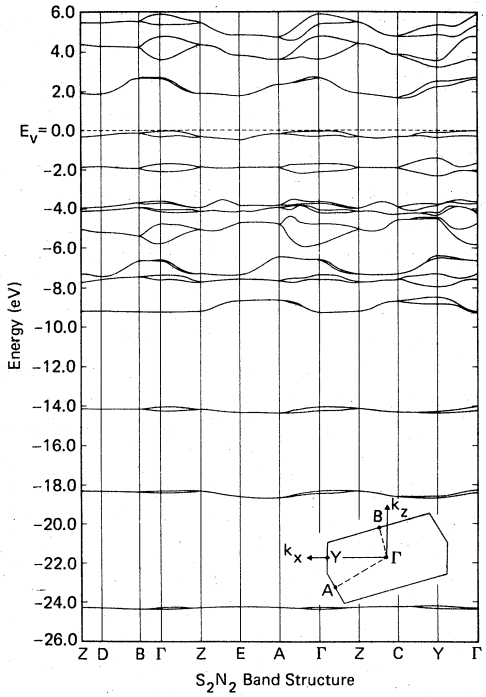

FIG. 7. Electronic energy band structure of S_2N_2 along various directions in the Brillouin zone. The insert shows the projection of the Brillouin zone in the $k_y = 0$ plane.

the structure provided by Cohen *et al.*[34] Each molecular unit is nearly square planar with essentially equal S-N bond lengths (~3.1 a.u.). It is believed[29,34] that due to the relatively short intermolecular S-N distance (~5.5 a.u.) along the crystallographic a axis, the polymerization takes place along this axis and it transforms into the b axis of $(SN)_x$. This is a very important point and is worthy of further examination. Furthermore, as a precursor to $(SN)_x$, a detailed electronic structure investigation of crystalline S_2N_2 is likely to provide insight into the properties of $(SN)_x$. This is the subject of the following discussion.

The electronic energy band structure for S_2N_2 along various directions in the Brillouin zone for the basis set (b) is shown in Fig. 7. The inset in Fig. 7 shows the projection of the brillouin zone in the $k_y = 0$ plane. The details of the calculation have been discussed above for $(SN)_x$ and are similar for S_2N_2. To our knowledge, this is the first time that the band structure of crystalline S_2N_2 has been reported [see note added in proof]. It is clear from Fig. 7 that most bands are narrow and nearly doubly degenerate due to relatively small interaction of various orbitals on the two molecular units. However at Γ point the set of levels 13,14; 19,20 and 21,22 are particular exceptions to this degeneracy rule. They are split apart in amounts ranging from 0.3–1.0 eV primarily due to interactions involving various sulfur atoms. These are also the levels which are dispersive (see Fig. 7). The two highest occupied levels 21, 22 at Γ correspond to essentially nonbonding S $3p_y$ orbitals. This is in agreement with the results obtained from S_2N_2 molecular studies[9,17] where the highest filled band corresponds to S p orbitals. The two lowest unoccupied pair of levels 23,24 at Γ arise from S $3p$ and N $2p$ hybridization.

It is also clear from Fig. 7 that most bands are nearly dispersionless. Some dispersion occurs along what corresponds to the crystallographic a axis (see for example $A\Gamma$ direction). This axis transforms[34-36] into the b axis (intrachain direction) of $(SN)_x$, and the $(SN)_x$ bands along this direction are highly dispersive (see ΓZ direction in Fig. 4). We find that S_2N_2 is an indirect-gap semiconductor whose valence-band maximum occurs

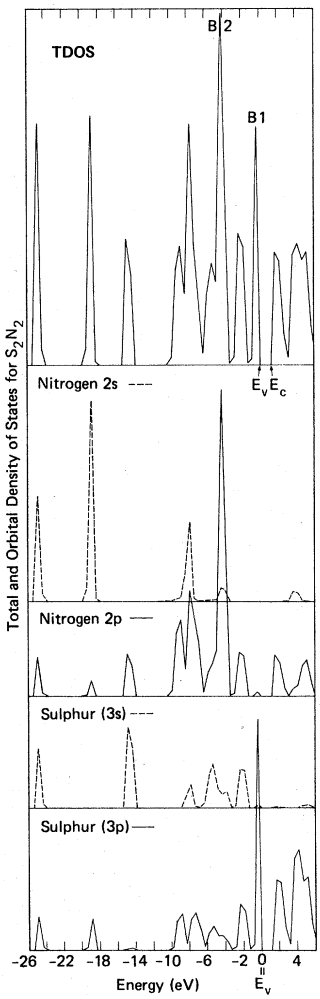

FIG. 8. Total and orbital density of states (normalized with respect to TDOS) for S_2N_2.

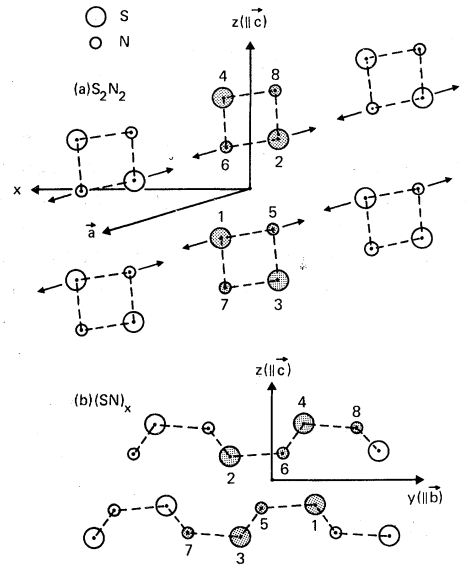

FIG. 9. (a) Projection of S_2N_2 in the xz plane. The crystallographic a axis and the direction of motion of the atoms necessary for polymerization are indicated by arrows, (b) projection of $(SN)_x$ in the yz plane. Shaded atoms are translationally inequivalent in the direct unit cell.

near the Γ point and the conduction-band minimum occurs near the C point in the Brillouin zone. The indirect energy gap is found to be about 1.7 eV and the direct gap at Γ is calculated to be 2.7 eV. We believe that these values are somewhat on the low side because thin films of S_2N_2 are essentially colorless,[29,34,36] and strong optical absorption[36] takes place around 4.0 eV. However, weak optical absorption[36] does take place below 3.0 eV, and in the absence of any knowledge about oscillator strengths, we are unable to reconcile the gap in the density of states with that observed[36] optically.

It is noted that the valence bandwidth for S_2N_2 (~24 eV) is quite comparable to $(SN)_x$. Therefore, the total electronic energy for the two materials would be nearly identical suggesting that both phases are equally stable. This seems to be consistent with the low heat of polymerization, which is measured[37] to be 3.7 kcal/mole of SN (S_2N_2 undergoes spontaneous exothermal polymerization). Calculations on isolated square planar S_2N_2 molecule have found values for the occupied valence level width ranging from[9,17] about 21–28 eV.[38]

To gain insight into the transition from the insulating S_2N_2 to metallic $(SN)_x$, we examine the orbital composition of various parts of the energy bands. A detailed examination of the orbital character of various bands across the entire Brillouin zone can be done in terms of total and orbital density of states shown in Fig. 8. This calculation was done for the basis set a to be consistent with the $(SN)_x$ calculation. As noted earlier there are no substantial differences between the two basis sets. Three lower-lying peaks primarily arise from N 2s and S 3s electrons. The p contribution starts to increase as one approaches the valence-band edge. Peaks labeled $B1$ and $B2$ have their origins in essentially nonbonding S 3p and N 2p electrons, respectively. It is clear that S_2N_2 has almost no overlap between S 3p and N 2p electrons near E_v. The novel structure of $(SN)_x$ does permit such an overlap. This important distinction will be used below to illustrate why the energy gap disappears in $(SN)_x$. To our knowledge there is no XPS or UPS data available for S_2N_2 at the present time. These should be worthwhile experiments to perform for elucidating the nature of transition from S_2N_2 to $(SN)_x$. We hope such experiments will soon be forthcoming.

To elucidate the transition from insulating S_2N_2

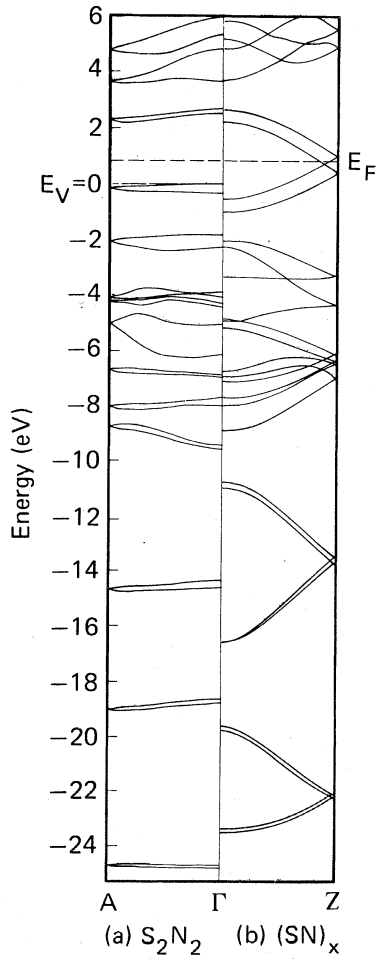

FIG. 10. Band structures of (a) S_2N_2 along ΓA direction and (b) $(SN)_x$ along ΓZ direction.

to metallic $(SN)_x$ we have shown the xz projection of S_2N_2 and yz projection of $(SN)_x$ in Fig. 9. The polymerization[29,34,35] along the a axis is schematically shown by indicating the direction of movement of atoms by small arrows. The band structures for S_2N_2 along the ΓA direction (i.e., the crystallographic a axis) for $(SN)_x$ along the ΓZ direction (i.e., the crystallographic b axis) are shown next to each other in Fig. 10. The Fermi levels for $(SN)_x$ and S_2N_2 (assumed located at the mid-energy gap) were aligned, and all energies are measured with respect to the valence-band edge ($E_v = 0$) of S_2N_2. In the intermediate energy range (−2 to −8 eV) somewhat less dispersive bands of S_2N_2 become more dispersive for the $(SN)_x$ structure. But in the lower energy range (−9 to −25 eV) and near the top of the filled band, relatively dispersionless pairs of doublets of S_2N_2 become highly dispersive and reach a near fourfold degeneracy at the Z point for $(SN)_x$. It is clear from Fig. 10 that the occurrence of this near fourfold degeneracy around E_F corresponds to a near degeneracy of the empty and occupied bands in $(SN)_x$ leading to metallic behavior.

To discuss the absence of energy gap in $(SN)_x$ in terms of bonding effects, we recall that the top of the filled band in S_2N_2 consisted of nonbonding S π levels (see Fig. 8). As seen in Fig. 4 due to the novel structure of $(SN)_x$, S $3p$ and N $2p$ hybridization takes place giving rise to a σ bond which lies slightly lower in energy than the nonbonding π levels of S_2N_2. Thus the occupied and unoccupied levels are nearly-degenerate and hence, the metallic behavior in $(SN)_x$. This point has been beautifully illustrated by Salahub and Messmer[17] by performing molecular calculations on square planar and open structures for S_2N_2.

Note added in proof. Professor C. C. Lin has kindly advised us that a calculation on S_2N_2 by W. Y. Ching, J. G. Harrison, and C. C. Lin has already been accepted by Phys. Rev. B (to be published). It is a pleasure to note that their results agree quite well with ours.

ACKNOWLEDGMENTS

The authors acknowledge useful discussions with Dr. P. S. Bagus, Dr. W. D. Gill, Dr. P. M. Grant, Dr. R. L. Greene, Dr. F. Herman, Dr. H. Morawitz, Dr. B. H. Schechtman, and Dr. G. B. Street.

*Permanent address: T.B.T.A.K. Marmara Scientific and Industrial Research Institute, Gebze-Kocaeli, Turkey.

[1]V. V. Walatka, M. M. Labes, and J. H. Perlstein, Phys. Rev. Lett. 31, 1139 (1973); C. Hsu and M. Labes, J. Chem. Phys. 61, 4640 (1974).

[2]R. L. Greene, P. M. Grant, and G. B. Street, Phys. Rev. Lett. 34, 89 (1975).

[3]A. A. Bright, M. J. Cohen, A. F. Garito, A. J. Heeger, C. M. Mikulski, and A. G. MacDiarmid, Appl. Phys. Lett. 26, 612 (1975).

[4]P. M. Grant, R. L. Greene, and G. B. Street, Phys. Rev. Lett. 35, 1743(C) (1975).

[5]R. L. Greene, G. B. Street, and L. J. Suter, Phys. Rev. Lett. 34, 577 (1975); G. B. Street, H. Arnal, W. D. Gill, P. M. Grant, and R. L. Greene, Mater. Res. Bull. 10, 877 (1975); R. L. Greene and G. B. Street, Chemistry and Physics of One Dimensional Metals (Plenum, New York, to be published).

[6]B. T. Matthias, Int. J. Quantum Chem. 10, 435 (1976).

[7]L. Pintschovius, H. P. Geserich, and W. Möller, Solid State Commun. 17, 477 (1975). For a review see, H. P. Geserich and L. Pintschovius, Adv. Solid State Phys. XVI, 65 (1976).

[8]See, for example, W. R. Salaneck, J. W-P. Lin, A. Paton, C. B. Duke, and G. P. Ceasar, Phys. Rev. B 13, 4517 (1976).

[9]D. R. Salahub and R. P. Messmer, J. Chem. Phys. 64, 2039 (1975); M. P. S. Collins and B. J. Duke, J. C. S. Chem. Commun. 17, 701 (1976).

[10]W. I. Friesen, A. J. Berlinsky, B. Bergersen, L. Weiler, and T. M. Rice, J. Phys. C 8, 3549 (1975).

[11]D. E. Parry and J. M. Thomas, J. Phys. C 8, L45 (1975).

[12]H. Kamimura, A. J. Grant, F. Levy, A. D. Yoffe, and G. D. Pitt, Solid State Commun. 17, 49 (1975); M. Kertész, J. Koller, A. Azman, and S. Suhai, Phys. Lett. A 55, 107 (1975); A. Zunger, J. Chem. Phys. 63, 4854 (1975); A. D. Yoffe, Chem. Soc. Rev. 5, 51 (1976).

[13]V. T. Rajan and L. M. Falicov, Phys. Rev. B 12, 1240 (1975).

[14]M. S. Schlüter, J. R. Chelikowsky, and M. L. Cohen, Phys. Rev. Lett. 35, 869 (1975); 36, 452 (1976).

[15]A. A. Bright and P. Soven, Solid State Commun. 18, 317 (1976).

[16]H. Kamimura, A. M. Glazer, A. J. Grant, Y. Natsume, M. Schreiber, and A. D. Yoffe, J. Phys. C 9, 291 (1976).

[17]R. P. Messmer and D. R. Salahub, Chem. Phys. Lett. 41, 73 (1976); D. R. Salahub and R. P. Messmer, Phys. Rev. B 14, 2592 (1976).

[18]W. E. Rudge and P. M. Grant, Phys. Rev. Lett. 35, 1799 (1975).

[19]W. Y. Ching and C. C. Lin, Bull. Am. Phys. Soc. 21, 254 (1976); and Phys. Rev. B (to be published).

[20]E. E. Lafon and C. C. Lin, Phys. Rev. 152, 579 (1966); R. C. Chaney, T. K. Tung, C. C. Lin, and E. E. Lafon, J. Chem. Phys. 52, 361 (1970); R. C. Chaney, E. E. Lafon, and C. C. Lin, Phys. Rev. B 4, 2734 (1971); W. Y. Ching and J. Callaway, *ibid.* 9, 5115 (1974); J. E. Simmons, C. C. Lin, D. F. Fouqnet, E. E. Lafon, and R. C. Chaney, J. Phys. C 3, 1549 (1975); U. Seth and R. C. Chaney, Phys. Rev. B 12, 5923 (1975).

[21]S. Ciraci and I. P. Batra, Phys. Rev. B 15, 3254 (1977); and Proceedings of the XIII International Con-

ference on the Physics of Semiconductors, Rome, August, 1976 (unpublished).
[22]R. H. Parmenter, Phys. Rev. 86, 552 (1952); W. Y. Ching and C. C. Lin, Phys. Rev. Lett. 34, 1223 (1975); R. C. Chaney (private communication).
[23]I. P. Batra and S. Ciraci, Proceedings of the Noordwijk Meeting on Photoemission from Surfaces, September 13–16, 1976 (unpublished).
[24]S. Ciraci and I. P. Batra, Phys. Rev. B (to be published).
[25]J. M. Andre, in *Proceedings of the International Symposium on Selected Topics in Molecular Physics* (Verlag Chemie, Berlin, 1970), p. 169; J. C. Callaway and J. L. Fry, *Computational Methods in Band Theory* (Plenum, New York, 1974), p. 512.
[26]E. Clementi and C. Roetti, At. Data Nucl. Data Tables 14, 177 (1974).
[27]S. F. Boys, Proc. R. Soc. Lond. Ser. A 200, 542 (1950); S. Huzinaga, J. Chem. Phys. 42, 1293 (1965); B. Roos and P. Siegbahn, Theor. Chim. Acta (Berlin) 17, 199 (1970).
[28]T. B. Grimley, J. Phys. C 3, 1934 (1970); I. P. Batra and C. R. Brundle, Surf. Sci. 57, 12 (1976); D. J. M. Fassaert and A. Van Der Avoird, *ibid.* 55, 291 (1976).
[29]C. M. Mikulski, P. J. Russo, M. S. Saran, A. G. MacDiarmid, A. F. Garito, and A. J. Heeger, J. Am. Chem. Soc. 97, 6358 (1975). An earlier structure using electron diffraction techniques by M. Boudeulle [Crystallogr. Struct. Commun. 4, 9 (1975)] is also available but may be slightly less accurate.
[30]L. Ley, Phys. Rev. Lett. 35, 1796 (1975).
[31]P. Mengel, P. M. Grant, W. E. Rudge, B. H. Schechtman, and D. W. Rice, Phys. Rev. Lett. 35, 1803 (1975).
[32]E. E. Koch and W. D. Grobman (unpublished).
[33]J. H. Scofield, Tables of Theoretical Photoionization Cross Sections, Lawrence Livermore Laboratory Report No. UCRL-51326 (1973) (unpublished).
[34]M. J. Cohen, A. F. Garito, A. J. Heeger, A. G. MacDiarmid, C. M. Mikulski, M. S. Saran, and J. Kleppinger, J. Am. Chem. Soc. 98, 3844 (1976).
[35]R. H. Baughman, R. R. Chance, and M. J. Cohen, J. Chem. Phys. 64, 1869 (1976).
[36]Z. Iqbal and D. S. Downs, Solid State Commun. 20, 1147 (1976).
[37]G. B. Street and R. L. Greene, IBM J. Res. Devel. 21, 99 (1977).
[38]M. Kertesz, S. Suhai, A. Azman, D. Kocjan, and A. I. Kiss, Chem. Phys. Lett. 44, 53 (1976).